# The occurrence frequency of upward ion beams in the auroral zone as a function of altitude using Polar/TIMAS and DE-1/EICS data

A. Olsson, P. Janhunen, W.K. Peterson

April 13, 2002

**Abstract**

We study the auroral upward ion beam occurrence frequency as a function of altitude using 5 years of Polar/TIMAS ion data combined with 11 years of DE-1/EICS ion data in order to reach a complete altitude coverage between 5000 and 30000 km. The most interesting result is that there is a peak in ion beam occurrence frequency and invariant energy and particle flux at $\sim$3 $R_E$ radial distance. On the topside of the peak there is a reduction of ion beam mean energy. The peak exists at about the same altitude in both evening and midnight MLT sectors and for small and large Kp's. No solar cycle effects are found. We suggest that the peak might be due to a preferred altitude of auroral potential structures at $\sim$3 $R_E$. Another result is that the ion beam occurrence frequency and invariant (mapped to ionospheric altitude) energy and particle fluxes increase in the radial distance range 4-6 $R_E$, suggesting that two-stream instability and wave heating processes may take place in this altitude range.

## 1 Introduction

Energetic, up to several kiloelectron volt, upward ion beams exist in auroral field lines, mainly in conjunction with optical auroral arcs and inverted-V electron precipitation. The first systematic studies of upward ion beams were made by the S3-3 satellite in the 1000-8000 km altitude range [*Gorney et al.,* 1981, *Collin et al.,* 1982, *Ghielmetti et al.,* 1978]. Somewhat later, DE-1 covered the 8000-24000 km altitude range, also giving rise to ion beam statistical studies [*Yau et al.,* 1984, *Yau et al.,* 1985a, *Yau et al.,* 1985b, *Kondo et al.,* 1990]. The Viking satellite covered the altitude region 2000-14000 km and gave rise to some event-based ion beam studies [*Lundin et al.,* 1987]. Lower altitude (1000-4000 km) ion beam studies have later been conducted with FAST [*Möbius et al.,* 1998, *McFadden et al.,* 1998, *McFadden et al.,* 1999]. Also Polar and Akebono have been used below 10000 km for low altitude studies of ion beams [*Collin et al.,* 1998, *Peterson et al.,* 1993]. Reviews of auroral zone ion populations have been given by *Peterson* (1988) and *André and Yau* (1997).

Upward moving ions can be energized by both waves and quasistatic electric fields. Thus, studying the ion beam energy and occurrence frequency as a function of altitude can give information on both waves and quasistatic parallel electric fields in the auroral region. The altitude dependence of ion beams has been studied statistically in the past by *Yau et al.* [1984] and *Kondo et al.* [1990], both using DE-1 data (8000-24000 km altitude range). The *Yau et al.* [1984] study uses 1981-82 data while *Kondo et al.* [1990] use 1981-86. A minimum in ion beam occurrence frequency for both oxygen and hydrogen was found at around 16000 km

altitude (except for energies less than 1 keV for which the occurrence frequency was monotonically increasing as a function of altitude). Studying this phenomenon further is one of the motivations for the present study.

We will study the altitude dependence of upward ion beams as a function of magnetic local time (MLT) and invariant latitude (ILAT) as well as for different Kp, solar illumination and solar cycle phase conditions. Previous results for ion beams, integrated over altitude and as a function of MLT, appeared in *Gorney et al.*[1981], Figure 3, and *Yau et al.*[1985b], Figure 8. The maximum number fluxes in $O^+$ ion beams were found to occur in the premidnight sector. In the 6000-8000 km altitude range, *Johnson* [1983] found that the maximum occurrence frequency is reached around MLT 18 for high Kp. Statistical plots of ILAT appeared in Figures 5,6 and 13 of *Yau et al.*(1984) and Figure 8 of *Yau et al.*(1985b), integrated over altitude. The low energy ion beam ILAT versus MLT dependence closely followed the ILAT vs. MLT dependence of the auroral oval. Seasonal dependence was studied by *Yau et al.*[1985a]. Their conclusion was that summer O+ fluxes were higher in the absolute sense than winter O+ fluxes when integrated over altitude, but no difference was seen in hydrogen. Regarding Kp dependence (Figure 5 of *Yau et al.*[1985b] and Figure 8 of *Kondo et al.*[1990]), it was found that the ion fluxes increase as a function of Kp in such a way that O+ fluxes increase more than H+ fluxes. Using one year of TIMAS data it has also been found that ion beams below 10000 km occur ~3 times more often during wintertime than during summertime [*Collin et al.,* 1998].

In this paper we study the ion beams statistically as a function of altitude using two different ion instruments, TIMAS and EICS, from two satellites, Polar and DE-1. The main reason for selecting Polar is the fact that it covers all altitudes above 5000 km, up to and exceeding 30000 km which we set as an upper limit of our study. The TIMAS instrument onboard Polar suffered a high-voltage breakdown on December 8, 1998 and thus the altitude coverage is incomplete. We use DE-1/EICS to complete the altitude coverage. DE-1/EICS is similar to TIMAS except that the time and energy resolutions are somewhat inferior. The main new thing to study is the altitude profile of ion beam occurrence frequency up to 30000 km and how the profile depends on MLT, ILAT, etc. We will also compute other statistical properties of ion beams to allow comparisons with previous works.

## 2 Instrumentation and data analysis

We use Polar/TIMAS for covering the altitude ranges 5000-10000 and 20000-32000 km during 1996-1998 [*Shelley et al.,* 1995]. TIMAS suffered a high-voltage breakdown in December 8, 1998 and experienced a loss of telemetry for portions of 1999, 2000 and 2001. Although TIMAS reinitiated routine operations on 30 March, 2001, the high-voltage breakdown of 1998 resulted in a loss of sensitivity that makes intercomparisons of statistical databases obtained before and after December 8, 1998 extremely challenging. We choose not to use TIMAS data acquired after December 8, 1998 in this analysis. This makes the altitude coverage of TIMAS incomplete. The EICS instrument onboard DE-1 made measurements 1981-1991 covering altitudes between 8000-23000 km [*Shelley et al.,* 1981]. Using both instruments together we can thus obtain a complete altitude coverage from 5000 km to 30000 km.

In order to be able to use Polar/TIMAS and DE-1/EICS in the same statistics, careful intercalibration is necessary. This will be addressed in section 2.4 ("Polar/TIMAS and DE-1/EICS intercomparison").

## 2.1 Data sets

The Polar/TIMAS instrument produces the differential energy flux for all pitch angles and energies with $15^o$ pitch angle bins and 28 logarithmically spaced energy steps between 15 eV and 33 keV every two satellite spins (about 12 s). Before June 1996 the upper energy limit was 25 keV, however. The data files used in this study are version 2 high resolution files from the online database of instrument data from many satellites provided by NASA on the CDAWeb site. The DE-1/EICS instrument is very similar to Polar/TIMAS. However, the time resolution of the CDAWeb data files we are using is 16 spins (96 s, i.e. 8 times lower time resolution than for Polar/TIMAS) and also the energy range is more restricted than TIMAS (10 eV to 17 keV). Our method for finding ion beams requires at least 2 energy channels above the peak energy, thus the maximum peak energy with DE-1/EICS is 10 keV. In order to compare the datasets with the same resolution and restrictions, both binning in time and energy range of the TIMAS data set are adjusted to the capabilities of EICS in our comparison.

The datasets we are using are the best existing from these instruments. The only compromise in the data quality in these sets is that gyrotropy has been assumed throughout, but this is no problem in the present study.

After this paper was written, an error was noticed in Polar/TIMAS telemetry processing which may affect the dayside flux values in the 10-14 MLT range. Consequently, the flux values in this MLT range appearing in Figures 8 and 9 below may be slightly in error. No conclusions are drawn in this paper concerning this MLT range.

## 2.2 Finding ion beams

We identify the ion beams as energy-angle structures by the following method based on Gaussian fitting. Ion beams are usually defined as maxima in phase space density, but we choose to define them as peaks in the differential energy flux. Let $F(E, \theta)$ denote the measured differential energy flux where $E$ is the energy and $\theta$ is the pitch angle. Upward ion beams are maxima of $F(E, \theta)$ appearing close to $\theta = \pi$ for northern hemisphere (for southern hemisphere they appear close to $\theta = 0$ which we mention here only once). Especially at higher altitude they are often superposed with a smooth background which is almost symmetric in up/down direction. For each energy step, to separate the background we first subtract the downgoing part from the upgoing part and replace possible negative values by zero after subtraction. We then find all local maxima along $\theta = \pi$. We consider only maxima that exceed the background by at least 50%. After locating the maximum, the 2-D region in energy and pitch angle around the maximum which belongs to the same ion beam is found. The criteria used here are such that only values that exceed the local background flux by at least 30% are eligible and the values must be decreasing as one moves away from the maximum. We also require that the differential energy flux is at least $10^5$ cm$^{-2}$ s$^{-1}$ sr$^{-1}$. A Gaussian function in energy and pitch angle is then fitted to the maximum region. If the chi-squared of the fit is larger than 1 the fit is rejected. The energy and number fluxes belonging to the maximum region are then computed, scaled by particle flux conservation in a magnetic flux tube to ionospheric altitude and saved. In the scaling to ionospheric altitude the value of the magnetic field is needed; this is taken from the Polar/MFE if available, otherwise the dipole model is used. In the rare event of having several eligible local maxima in energy we select the one with the largest number flux. The processing of TIMAS and EICS data is identical except for the different energy grids.

We use several criteria to protect ourselves against different types of data errors. Passages of data with known instrument errors are removed. A data point is

excluded if the integrated energy flux (scaled to ionospheric altitude) exceeds $10^4$ mW m$^{-2}$ or if the number flux (also scaled to ionospheric altitude) exceeds $10^{14}$ m$^{-2}$ s$^{-1}$. These values are too high to be realistic (physical energy fluxes values may reach a few hundred mW m$^{-2}$ at most) and must correspond to erroneous flux values. Between April 1, 1996 and December 8, 1998, Polar/TIMAS had 23.9 days worth of valid nightside auroral crossing data (ILAT=65..74) and 27 days worth of missing data. The number of bad data points was only 2 (corresponding to total time 24 s). For DE-1/EICS, the percentage of bad data points is 0.9% and the total amount of nightside auroral zone time 59 days.

We limit ourselves only to invariant energy fluxes above 0.2 mW m$^{-2}$ and to ion beam energies in the range from 0.5 keV to 10 keV. By invariant energy and particle flux we mean that the quantities are projected to the ionospheric level. No distinction between ion species is made. A further condition that we use is that the integrated energy flux must be upward at the time of the ion beam, otherwise the beam is rejected.

## 2.3 Computation of occurrence frequencies

We want to compute the ion beam occurrence frequency as a function of different variables, among which are the radial distance $R$, the invariant latitude (ILAT), the magnetic local time (MLT), the Kp index value and solar illumination condition (i.e., whether the ionospheric footpoint is illuminated or not). We do not have enough orbital coverage to get the occurrence frequency in the whole five-dimensional array, however, neither would it be practical to plot. Instead, we typically display the dependence of the occurrence frequency on one of the important parameters, as a function of radial distance and averaged over all ILAT. There are in principle two ways to gather the statistics, (1) one puts all data points in the radial bin together and computes the occurrence frequency for them, (2) one calculates the occurrence frequency separately for each ILAT bin and computes the arithmetic average of the occurrence frequencies. Method (1) yields longer data vectors and thus smaller statistical uncertainties, but is vulnerable to possibly nonuniform orbital coverage in ILAT. Method (2) does not require uniform ILAT coverage, but gives larger statistical uncertainties if at least one of the ILAT bins contains significantly smaller number of data points as the other bins. If $f_i$ is the occurrence frequency in $i$th ILAT bin and $\sigma_i^2$ is the corresponding variance, the standard deviation of the whole radial bin is given by $(1/n)\sqrt{\sum_i \sigma_i^2}$ where $n$ is the number of ILAT bins (9 in our case).

We choose to use method (2) in this paper, with the additional assumption that if one of the ILAT bins has less than 100 measurements, it is dropped from the statistics so that it does not contribute to the total standard deviation. This is to handle in a meaningful way also cases where the ILAT coverage is otherwise good but there is lack of coverage close to one of the boundaries, where ion beams are rarely detected anyway.

## 2.4 Polar/TIMAS and DE-1/EICS intercomparison

The top panel of Figure 1 shows all ion beams between 0.5 and 10 keV as a function of radial distance $R$ and beam peak energy for conditions where the satellite ionospheric footpoint is sunlit. The left panel shows TIMAS results and the right panel EICS. Since the peak energy is quantized to one of the detector energy channel center energies, to ease plotting a uniform random number in the range $-0.5..0.5$ keV has been added to the ordinate of each data point. Since TIMAS files have 8 times higher time resolution than EICS, each EICS point is replicated 8 times in the upper right panel of Figures 1 and 2 to make the number of TIMAS and EICS

points mutually comparable. Comparison of the left and right panels of Figure 1 shows that the resulting occurrence frequencies agree relatively well in those altitude bins where both instruments have coverage. Figure 2 shows the corresponding result for conditions where the satellite ionospheric footpoint is in darkness. Also here TIMAS and EICS ion beam occurrence frequencies are in agreement in those altitude bins where both instruments have proper coverage.

To compare TIMAS and EICS results more quantitatively we decompose the statistics in the three nightside MLT sectors 18-22, 22-02 and 02-06. Table 1 shows the MLT-decomposed TIMAS and EICS occurrence frequencies for radial distance ranges 2-2.5 $R_E$ and 4-4.5 $R_E$ for sunlit cases and for Kp $>$ 2. The standard deviation error estimates are also given. Table 2 shows the corresponding comparison for darkness cases. In some cases which are noted in Table 2 we carry out the comparison for Kp $\leq$ 2, however, because of better orbital coverage and thus smaller statistical uncertainty. From the tables we see that in cases where orbital coverage allows comparison, the two satellites produce occurrence frequencies that in all cases except one are within the error limits of each other. The case not in perfect agreement is darkness MLT 22-02, 4-4.5 $R_E$ radial distance bin where the occurrence frequencies differ by 35%, or 5 standard deviations. Since our *a priori* standard deviation only takes into account the statistical noise due to a finite number of data points but not the temporal correlations of ion beams, it is not unexpected that in some cases the values are a few standard deviations away from each other. Thus the true statistical errors are somewhat larger than the *a priori* standard deviations, which are based on the number of data points. We shall call estimates of the true statistical errors the *a posteriori* standard deviations.

Let us estimate the *a posteriori* standard deviation for the calibration bins. There are 10 bins, in nine of which the two satellites agree within the *a priori* standard deviations, but in one bin the discrepancy is 5 *a priori* standard deviations. If the *a posteriori* standard deviation is $\sigma$, we can write the average variance per data point as $(9 \times (1/\sigma)^2 + 1 \times (5/\sigma)^2)/10$. If we require that this expression has the value 1 and solve for $\sigma$ we obtain $\sigma = 1.84391$. We adopt this value as our a relative posteriori standard deviation. Henceforth in all plots shown, the displayed error bars are the *a posteriori* error bars, i.e. the $1/\sqrt{n}$ *a priori* error estimates multiplied by $\sigma$.

We conclude that TIMAS and EICS data agree well enough so that when the ion beams are found and the error bars drawn in the manner described above, data from both satellites can be put in the same statistics.

# 3 Results

## 3.1 Radial distance

In Figure 3 we show our baseline plot, which is TIMAS and EICS ion beams put together in the 0.5-10 keV energy range for all nightside MLT sectors and sunlit and darkness conditions. The occurrence frequency of ion beams generally increases with altitude, but there is also a relative maximum in the occurrence frequency of ion beams at 3 $R_E$ radial distance. In the baseline case (dotted line in Figure 3 representing all Kp's put together), the relative maximum (henceforth called "the peak") occurs at 2.75 $R_E$ radial distance and a local minimum at 3.75 $R_E$. The existence of a peak can be seen in earlier plots [*Gorney et al.,* 1981, *Yau et al.,* 1985b] but it has not been discussed.

### 3.2 Kp

Figure 3 shows small Kp ($\leq 2$) by filled circles and large Kp ($> 2$) by triangles. The combined statistics are shown by dotted line. Generally the ion beam occurrence frequency is ~2-3 times larger for Kp $> 2$ than for Kp $\leq 2$. The peak and the minimum above it occur at a lower radial distance for small Kp (2.75 and 3.25 $R_E$, respectively) than for large Kp (3.25 and 3.75 $R_E$).

### 3.3 MLT and solar illumination

In Figure 4 we show the ion beam statistics separated into three nightside MLT sectors and sunlit (top) and darkness (bottom) conditions. Comparing radial distance bins below 2.5 $R_E$ for high Kp conditions, the occurrence frequency in darkness is 0.05 which is 2.5 times higher than in sunlit conditions in the evening sector (18-22 MLT). Overall this is in agreement with a previous study where a ratio $\sim 3$ was found in the occurrence frequency in darkness versus sunlit beams [*Collin et al.,* 1998], although the beam selection criteria and thus the absolute occurrence frequencies are different in the two studies. It is also seen that between 2.5 and 3.5 $R_E$ the occurrence rate of ion beams is higher during darkness than during sunlit conditions, although the difference is not as large as below 2.5 $R_E$.

The relative peak in occurrence frequency around 3 $R_E$ radial distance is most apparent in the evening sector (18-22 MLT). In this sector we also have the best overall orbital coverage so that the statistical errors are the smallest. In the morning sector there is no orbital coverage at all close to 3 $R_E$ so the existence of the peak remains uncertain in that MLT sector. In the evening sector and for small Kp, the occurrence frequency radial peak becomes wider in darkness as compared to sunlit conditions. For large Kp such difference is not clearly seen.

Ion beams for small Kp are rare in other MLT sectors except the midnight sector where they are almost equally common for small and large Kp indices.

### 3.4 Solar cycle effects

In Figure 5 we show the statistics separated into solar minimum (left panel) and solar maximum years (right panel). We take years 1978-1982, 1988-1992 and 1999- to be solar maximum years. Other years are taken to be solar minimum. Thus TIMAS (1996-1998) contributes to the solar minimum statistics only. There is hardly any systematic dependence on the solar cycle. From the orbital coverage panels one sees that during solar maximum years, high Kp values are always more common than small Kp values while for solar minimum years they are about equally common, which is not surprising.

### 3.5 ILAT dependence

To investigate ILAT dependence, we show in Figure 6 the occurrence frequency for all nightside MLT but decomposed into three ILAT ranges: 65-68 (bottom panel), 68-71 (middle panel) and 71-74 (top panel). We see that small Kp events occur only seldom below ILAT 68, which is natural. The occurrence frequency is largest in the 68-71 ILAT bin, which corresponds to the average auroral oval latitudes. The peak is seen to exist at all ILAT ranges separately. For high ILAT, high Kp values behave similarly to low Kp values as far as the position of the peak is concerned, having similarly low peak position (2.75 $R_E$) as is typical for low Kp. It may be so that the determining variable is ILAT rather than Kp: the fact that the peak altitude is low for small Kp might be due to the fact that during low Kp, northward interplanetary magnetic field (IMF) often persists and auroras occur at higher ILAT than during more disturbed conditions.

Another wiew to the ILAT dependence is provided in Figure 7, which shows the two-dimensional ILAT-altitude statistics of all nightside ion beams. At both high and low altitude where the orbital coverage is good, most ion beams are seen around 70° ILAT.

In Figures 8 and 9 we show that statistics in the MLT-ILAT plane and MLT-$R$ plane, respectively. In the MLT-ILAT plane the auroral dependence of ion beams is clearly seen, i.e. that beams occur at lowest ILAT close to midnight and that they occur most often near midnight, with a slight preference for premidnight. In Figure 9 the auroral dependence can be seen as well, together with the fact that the $\sim 3$ $R_E$ occurrence frequency peak is visible in essentially all MLT sectors where there is orbital coverage and ion beams.

From Figure 8 one sees that ion beams, when all altitudes are put together, occur mostly in the 22-24 MLT sector, in accordance with the results of [*Yau et al.,* 1985b] and [*Gorney et al.,* 1985], whereas *Johnson* [1983] in his Figure 5 found that ion beams, at least during disturbed conditions, occur mostly in the 15-21 MLT range. The results of *Johnson* [1983] represent the altitude range 6000-8000 km only, however, which corresponds to our second altitude bin (2-2.5 $R_E$ radial distance). Inspection of Figure 4 shows that in this altitude bin, ion beams for large Kp are indeed much more common in the 18-22 than in the 22-02 MLT sector in our database. Thus our results are in agreement also with those of *Johnson* [1983]. Thus, at low altitude and high Kp, ion beams are mainly an evening sector phenomenon, while at high altitude and low Kp they are more a midnight sector phenomenon.

### 3.6 Ion beam energy flux and ion energies

From what we have shown we now know that most low altitude ion beams occur in the evening sector and high altitude ion beams mainly in the premidnight sector. Thus far we have only considered the occurrence frequency of ion beams, but now we will study the energy and particle fluxes carried by the beams. In Figure 10 we show the invariant energy flux in mW m$^{-2}$ and the invariant particles flux in m$^{-2}$ s$^{-1}$ carried by the upward ion beams. Both quantities are altitude-invariant in the sense that they have been projected to the ionospheric plane by multiplying them by the magnetic field ratio. They have been averaged linearly over all data points. Regions where no ion beams are detected are assumed to have zero energy and particle flux, thus the quantities plotted tell how much energy and particle flux is carried away from the ionosphere by ion beams on the average in the 65-74 ILAT range and 18-22 MLT.

If all ion beams could be reliably detected and if there were no wave-particle interactions, the conservation of beam particles would dictate that the invariant particle flux should be independent of altitude. From the third panel of Figure 10 we see that this is clearly not the case, but the invariant number flux generally increases with altitude. Thus, if we exclude instrumental effects for a moment (they will be discussed in the Discussion section below), it must be that new particles enter pre-existing beams at all altitudes, or that new beams are initiated also at intermediate altitudes, or both.

The invariant energy flux altitude trend largely follows the particle flux trend. If the only energization mechanism were a potential drop acceleration below 8000 km, say, the invariant energy flux should stay constant above 8000 km ($R = 2.25R_E$). This is not the case, but the invariant energy flux increases, which suggests that wave heating also plays a role. In the fourth panel of Figure 10 we show the mean energy of ion beams, computed as a weighted average of detected ion beams using the particle fluxes as weights. No clear trends are seen in the mean energy, which reflects the fact that the invariant energy and particle fluxes have rather similar altitude profiles. We shall return to the question of ion beam energization

mechanisms at different altitudes in the Discussion section.

In addition to the generally increasing trend of invariant energy and particle fluxes with altitude, we see from Figure 10 that the 3 $R_E$ peak appears also in the averaged energy and particle fluxes, not only in the ion beam occurrence frequency. In the 3.25 $R_E$ radial distance bin there is a decrease of the mean energy (Figure 10, fourth panel).

Here we discussed only the evening sector. Similar trends in the invariant energy and particle fluxes and ion mean energy exist in the midnight sector, although they are less pronounced.

# 4 Discussion

In this study we have confirmed previous results such as the fact that ion beams occur less often in the morning sector than in the evening and midnight sectors and that low altitude beams ($< 2.5R_E$) occur more often when the ionosphere is in darkness than when it is illuminated by sun. Also the result that ion beam occurrence frequency increases with increasing Kp index is in accordance with previous studies.

The most interesting result is that there is a peak in occurrence frequency at $\sim$3 $R_E$ radial distance. The peak can also be seen as a enhancement in invariant energy and particle fluxes and its topside as a reduction in mean ion energy. A peak in occurrence frequency can be seen in earlier plots (Yau et al, 1984, Figure 4 right panel; Kondo, 1990, Figure 7 right panel; Peterson et al., 1992, Figure 2 topleft panel), but it has not been investigated more closely. These earlier studies use DE-1 data, which in our case is the only contributor at the peak altitude, so the earlier results are in this sense not independent from ours, although our use of Polar data in this study has allowed us to validate DE-1 data at low and high altitude. Another result is an increase in ion beam occurrence frequency for $R > 4R_E$; this result is not possible to obtain with DE-1 alone because DE-1 apogee radial distance is 4.5 $R_E$. We will now itemize our main results:

1. In the baseline case (all MLT, ILAT, Kp and solar illuminations conditions put together), a peak in occurrence frequency of ion beams exists at 2.75 $R_E$ radial distance, and a local minimum occurrence frequency above it at 3.75 $R_E$.

2. The peak in occurrence frequency of ion beams and the minimum above it are raised to higher altitude with increasing Kp index.

3. When considering low and high Kp separately, the solar cycle does not have a notable influence on the ion beam occurrence frequency.

4. A peak is also present in the invariant energy and particle fluxes carried by upward ion beams, where "invariant" means that both quantities are projected to the ionospheric plane. The mean ion energy is locally reduced at the topside of the peak.

5. The peak appears in all ILAT ranges, but is most visible in the 68-71 ILAT bin, probably because that corresponds to the average auroral oval latitude.

6. At low altitude and high Kp, ion beams are mainly an evening sector phenomenon, while at high altitude and low Kp they are more a midnight sector phenomenon. The reasons for this remain unknown, but would deserve to be studied further.

7. The ion beam occurrence frequency and invariant energy and particle fluxes (invariant means that they are mapped to ionospheric altitude) continue to increase at high altitude ($R > 4R_E$). They do so in such a manner that their ratio (the mean energy) stays approximately constant.

We will now discuss two instrumental explanation attempts for the peak seen in the occurrence frequency of ion beams and rule them out one by one:

1. The flux tube scaling dictates that the number flux of an ion beam with ionospheric origin will decay as $R^{-3}$. This implies that weak beams fall below the instrument threshold from some altitude upwards. The depression above the 3 $R_E$ occurrence frequency peak is too sharp to be explained by this mechanism, however. Furthermore, the mechanism would not explain why the occurrence frequency increases again at even higher altitudes.

2. The peak does not disappear when the data are studied separately for different geomagnetic disturbance level (Kp index), solar cycle phase, solar illumination condition, magnetic local time and invariant latitude. This rules out the possibility that the peak could be due to some instrumental problem that persisted in a certain time period.

Beam ions are likely to be energized by both auroral potential structures and waves. This is already evident from the fact that one often sees ion beams of 10-20 keV energy in TIMAS data (even energies as high as 40 keV have been reported [*Lundin and Eliasson,* 1991]), while potential structures of comparable magnitude are rare [*Olsson et al.,* 1998, *Janhunen et al.,* 2002]. Also the fact that the ion beam occurrence frequency as well as invariant number and energy fluxes continue to increase at high altitudes ($R > 4R_E$) suggests that there is continuous wave-induced ion heating or parallel electric fields at high altitude.

For wave heating to explain the increase in ion beam invariant energy and particle flux at high altitude, there are two possibilities. The first possibility is that cold background plasma existing at $R = 3R_E$, say, [*Peterson et al.,* 1993] receives perpendicular wave heating e.g. due to an onset of auroral activity and develops an ion conic [*Peterson et al.,* 1992, *André and Yau,* 1997], which at even higher altitude turns into a beam because of the mirror force.

The second possibility for explaining the increase in energy and particle flux at high altitude is that a normal ion beam that was generated at low altitude when flowing through a stationary cold background ion population interacts with the background by the two-stream instability [*André,* 1985]. A rather similar mechanism has been suggested to operate between different ion species of a single ion beam [*Möbius et al.,* 1998]. The net result of the process is a reduction of the mean energy and an increase of the number flux of the beam (the beam becomes "mass-loaded" with additional ions). Simultaneous perpendicular wave energization could increase of the upward invariant energy flux, reducing or even cancelling the reduction in mean energy.

As mentioned above, upward parallel electric fields at high ($R > 4R_E$) altitude are in principle also a possibility to explain ion beam energization at that altitude range, but this explanation is rather unlikely as we are not aware of inverted-V electron signatures at that altitude, at least not with keV energies. Also, the parallel electric field would have to be combined with the two-stream instability or other mechanisms to explain the increase of the invariant particle flux with altitude.

We now discuss how one could possibly explain the peak at $\sim 3\ R_E$ which is present in occurrence frequency, average energy flux and average particle flux carried by ion beams. Equivalently, one can speak of a minimum in these quantities occurring at $\sim 3.75 R_E$. At this point, some of the upgoing ion beams must change

their character so that they are not detected as beams. One possibility would be rapid wave-induced perpendicular heating that would turn the beams into conics, since conics are sometimes observed at this altitude [*Klumpar et al.,* 1984]. At higher altitude the mirror force would turn them into beams again, with much increased energy. Another possibility is that the ion beams slow down at this altitude by a downward electric field and thus some of them fall below the 0.5 keV threshold. A slowing down of the parallel velocity would give the ions more time to spend in this region, thus increasing the potential of perpendicular wave heating, so the disappearance of the beams could be partly caused by slowing down, partly from turning into conics and perhaps partly from being reflected downward by the downward field. The fact that the mean beam energy drops at the 3.25 $R_E$ radial bin (Figure 10, fourth panel) is compatible with slowing down by an electric field. An analogous process operating in the return current region below 7000 km altitude has been discussed earlier [*Gorney et al.,* 1985]. The possibility for a downward field in the 15000-20000 km altitude range has been invoked as one of the possibilities when trying to understand counterstreaming ions [*Sagawa et al.,* 1987, *Horita et al.,* 1987]. Later, a downward electric field in the 3-4 $R_E$ radial range has also been proposed as an explanation for the lack of auroral potential structures above 4 $R_E$ radial distance [*Janhunen et al.,* 1999, *Janhunen and Olsson,* 2000]. To resolve this question, more statistical studies of parameters other than ion beams (such as auroral potential structures, density cavities, waves and ion conics) are needed in the 2-4 $R_E$ radial distance range.

Acknowledgements. The work of AO is supported by the Swedish Research Council and that of PJ by the Academy of Finland. TIMAS data were produced under support of NASA contract NAG-53032 to Lockheed Martin and NAG5-11391 to the University of Colorado. We are grateful to NASA for making TIMAS data available through CDAWeb.

# References

[*André,* 1985] André, M., Ion waves generated by streaming particles, *Ann. Geophysicae,* 3. 73–80, 1985.

[*André and Yau,* 1997] André, M. and A. Yau, Theories and observations of ion energization and outflow in the high latitude magnetosphere, *Space Sci. Rev.,* 80, 27–48, 1997.

[*Collin et al.,* 1982] Collin, H.L., R.D. Sharp, and E.G. Shelley, The occurrence and characteristics of electron beams over the polar regions, *J. Geophys. Res., 87,* 7504–7511, 1982.

[*Collin et al.,* 1998] Collin, H.L., W.K. Peterson, O.W. Lennartsson, and J.F. Drake, The seasonal variation of auroral ion beams, *Geophys. Res. Lett., 25,* 4071–4074, 1998.

[*Ghielmetti et al.,* 1978] Ghielmetti, A.G., R.G. Johnson, R.D. Sharp and E.G. Shelley, The latitudinal, diurnal, and altitudinal distribution of upward flowing energetic ions of ionospheric origin, *Geophys. Res. Lett., 5,* 59–62, 1978.

[*Gorney et al.,* 1981] Gorney, D.J., A. Clarke, D. Croley, J. Fennell, J. Luhmann, and P. Mizera, The distribution of ion beams and conics below 8000 km, *J. Geophys. Res., 86,* 83–89, 1981.

[*Gorney et al.,* 1985] Gorney, D.J., Y.T. Chiu and D.R. Croley, Jr., Trapping of ion conics by downward parallel electric fields, *J. Geophys. Res., 90,* 4205–4210, 1985.

[*Horita et al.,* 1987] Horita, R.E., E. Ungstrup, E.G. Shelley, R.R. Anderson and R.J. Fitzenreiter, Counterstreaming ion events in the magnetosphere, *J. Geophys. Res., 92,* 13523–13536, 1987.

[*Janhunen et al.,* 1999] Janhunen, P., A. Olsson, F.S. Mozer and H. Laakso, How does the U-shaped potential close above the acceleration region? A study using Polar data, *Ann. Geophysicae,* 17, 1276–1283, 1999.

[*Janhunen and Olsson,* 2000] Janhunen, P. and A. Olsson, New model for auroral acceleration: O-shaped potential structure cooperating with waves, *Ann. Geophysicae,* 18, 596–607, 2000.

[*Janhunen et al.,* 2002] Janhunen, P., A. Olsson and H. Laakso, The occurrence frequency of auroral potential structures as a function of altitude using Polar/EFI data, *Ann. Geophysicae,* submitted, 2002.

[*Johnson,* 1983] Johnson, R.G., That hot ion composition, energy, and pitch angle characteristics above the auroral zone ionosphere, in High-latitude space plasma physics, pp. 271–294, ed. by B. Hultqvist and T. Hagfors, Plenum, New York, 1983.

[*Klumpar et al.,* 1984] Klumpar, D.M., W.K. Peterson and E.G. Shelley, Direct evidence for two-stage (bimodal) acceleration of ionospheric ions, *J. Geophys. Res., 89,* 10779–10787., 1984.

[*Kondo et al.,* 1990] Kondo, T., B.A. Whalen, and A.W. Yau, Statistical analysis of upflowing ion beam and conic distributions at DE 1 altitudes, *J. Geophys. Res., 95,* 12091–12102, 1990.

[*Lundin et al.,* 1987] Lundin, R., L. Eliasson, B. Hultqvist and K. Stasiewicz, Plasma energization on auroral field lines as observed by the Viking spacecraft, *Geophys. Res. Lett., 14,* 443–446, 1987.

[*Lundin and Eliasson,* 1991] Lundin, R. and L. Eliasson, Auroral energization processes, *Ann. Geophys., 9,* 202–223, 1991.

[*McFadden et al.,* 1998] McFadden, J.P., *et al.*, Spatial structure and gradients of ion beams observed by FAST, *Geophys. Res. Lett., 25,* 2021–2024, 1998.

[*McFadden et al.,* 1999] McFadden, J.P., C.W. Carlson, R.E. Ergun, D.M. Klumpar, and E. Moebius, Ion and electron characteristics in auroral density cavities associated with ion beams: No evidence for cold ionospheric plasma, *J. Geophys. Res., 104,* 14671–14682, 1999.

[*Möbius et al.,* 1998] Möbius, E., *et al.*, Species dependent energies in upward directed ion beams over auroral arcs as observed with FAST TEAMS, *Geophys. Res. Lett., 25,* 2029–2032, 1998.

[*Olsson et al.,* 1998] Olsson, A., Andersson, L., Eriksson, A.I., Clemmons, J., Erlandsson, R.E., Reeves, G., Hughes, T. and Murphree, J.S., Freja studies of the current-voltage relation in substorm related events, *J. Geophys. Res.,* 103, 4285–4301, 1998.

[*Peterson,* 1988] Peterson, W.K., Auroral zone ion composition, in: *Modeling magnetospheric plasma*, AGU, Washington, DC, 1988.

[*Peterson et al.,* 1992] Peterson, W.K., H.L. Collin, M.F. Doherty and C.M. Bjorklund, O+ and He+ restricted and extended (bi-modal) ion conic distributions, *Geophys. Res. Lett., 19,,* 1439–1442, 1992.

[*Peterson et al.,* 1993] Peterson, W.K., A.W. Yau and B.A. Whalen, Simultaneous observations of H+ and O+ ions at two altitudes by the Akebono and Dynamics Explorer 1 satellites, *J. Geophys. Res., 98,* 11177–11190, 1993.

[*Press et al.,* 1992] Press, W.H., S.A. Teukolsky, W.T. Vetterling and B.P. Flannery, Numerical Recipes in C, The art of scientific computing, 2nd ed., Cambridge, 1992.

[*Sagawa et al.,* 1987] Sagawa, E., A.W. Yau, B.A. Whalen and W.K. Peterson, Pitch angle distributions of low-energy ions in the near-earth magnetosphere, *J. Geophys. Res., 92,* 12241–12254, 1987.

[*Shelley et al.,* 1981] Shelley, E.G., D.A. Simpson, T.C. Saunders, E. Hertzberg, H. Balsiger and A.G. Ghielmetti, The energetic ion composition spectrometer (EICS) for the Dynamics Explorer-A, *Space Sci. Instrum.,* 5, 443, 1981.

[*Shelley et al.,* 1995] Shelley, E.G., A.G. Ghielmetti, H. Balsiger, R.K. Black, J.A. Bowles, R.P. Bowman, O. Bratschi, J.L. Burch, C.W. Carlson, A.J. Coker, J.F. Drake, J. Fischer, J. Geiss, A. Johnstone, D.L. Kloza, O.W. Lennartsson, A.L. Magoncelli, G. Paschmann, W.K. Peterson, H. Rosenbauer, T.C. Sanders, M. Steinacher, D.M. Walton, B.A. Whalen and D.T. Young, The Toroidal Imaging Mass-Angle Spectrograph (TIMAS) for the Polar Mission, Space Science Rev., 71, 1-4, 1995.

[*Yau et al.,* 1984] Yau, A.W., B.A. Whalen, W.K. Peterson, and E.G. Shelley, Distribution of upflowing ionospheric ions in the high-altitude polar cap and auroral ionosphere, *J. Geophys. Res., 89,* 5507–5522, 1984.

[*Yau et al.,* 1985a] Yau, A.W., P.H. Beckwith, W.K. Peterson, and E.G. Shelley, Long-term (solar cycle) and seasonal variations of upflowing ionospheric ion events at DE 1 altitudes, *J. Geophys. Res., 90,* 6395–6407, 1985.

[*Yau et al.,* 1985b] Yau, A.W., E.G. Shelley, W.K. Peterson, and L. Lenchyshyn, Energetic auroral and polar ion outflow at DE 1 altitudes: magnitude, composition, magnetic activity dependence, and long-term variations, *J. Geophys. Res., 90,* 8417–8432, 1985.

Table 1: TIMAS and EICS high Kp ion beam occurrence frequency when footpoint is sunlit

| | MLT 18-22 | MLT 22-02 | MLT 02-06 |
|---|---|---|---|
| TIMAS 2-2.5 $R_E$ | $0.016 \pm 0.005$ | - | - |
| EICS 2-2.5 $R_E$ | $0.022 \pm 0.004$ | - | - |
| TIMAS 4-4.5 $R_E$ | $0.055 \pm 0.006$ | $0.045 \pm 0.009$ | $0.016 \pm 0.008$ |
| EICS 4-4.5 $R_E$ | $0.056 \pm 0.005$ | $0.042 \pm 0.009$ | $0.01 \pm 0.001$ |

Table 2: TIMAS and EICS ion beam occurrence frequency when footpoint is in darkness; for high Kp conditions except when noted otherwise

| | MLT 18-22 | MLT 22-02 | MLT 02-06 |
|---|---|---|---|
| TIMAS 2-2.5 $R_E$ | $0.053 \pm 0.012$ | $0.018 \pm 0.0015$ | - |
| EICS 2-2.5 $R_E$ | $0.044 \pm 0.006$ | - | - |
| TIMAS 4-4.5 $R_E$ | $0.008 \pm 0.002$ (low Kp) | $0.088 \pm 0.005$ | $0.025 \pm 0.015$ |
| EICS 4-4.5 $R_E$ | $0.012 \pm 0.004$ (low Kp) | $0.073 \pm 0.001$ | $0.03 \pm 0.001$ |
| TIMAS 4.5-5 $R_E$ | $0.055 \pm 0.007$ | $0.075 \pm 0.001$ | $0.015 \pm 0.001$ (low Kp) |
| EICS 4.5-5 $R_E$ | - | $0.073 \pm 0.001$ | $0.016 \pm 0.001$ (low Kp) |

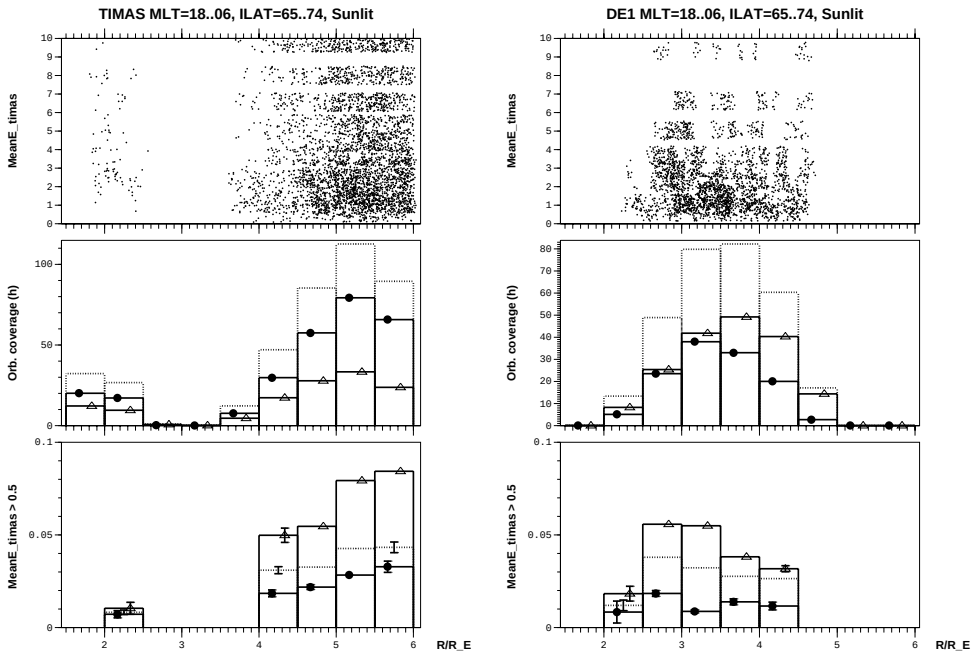


Figure 1: TIMAS (left), DE-1 (right). Top: All detected 0.5-10 keV beams as function of radial distance $R$ ($R_E$) and beam peak energy. Middle: Hours spent by the instrument in each bin. Bottom: Occurrence frequency of ion beams (number of points in each bin divided by the number of 12-s samples coming from the bin, averaged over ILAT). Small Kp ($\leq 2$) shown by filled circles, large Kp ($> 2$) by triangles. Dotted line is both Kp's put together. All nightside MLT sectors (18-06) are included and the satellite footpoint is sun-illuminated. Error bars are shown when they are significant.

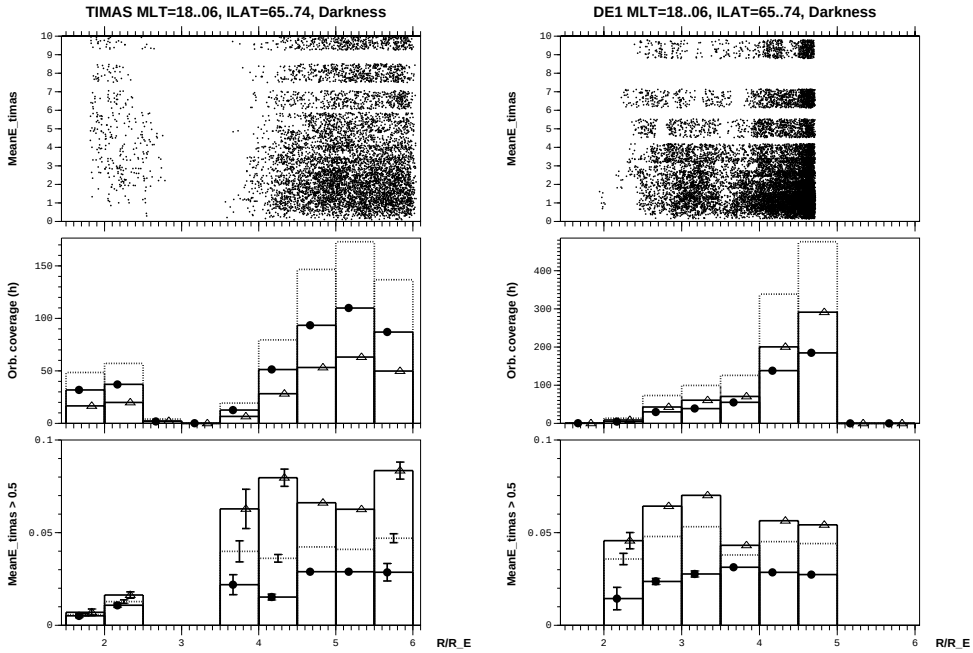


Figure 2: Same as Figure 1 but for conditions when the satellite footpoint is in darkness.

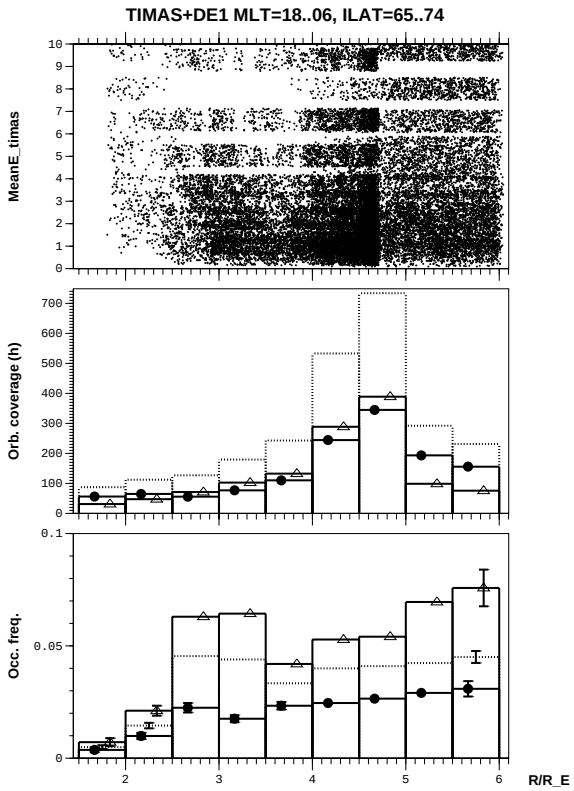


Figure 3: TIMAS and EICS ion beams in the nightside MLT sectors as a function of radial distance $R$. Top panel: Ion beam events (one event corresponds to 12 s sample) as function of radial distance and peak energy. Middle panel: Hours spent by the instrument in each radial bin. Bottom panel: Occurrence frequency of ion beams (number of points in each bin divided by the number of samples coming from the bin). Small Kp ($\leq 2$) shown by filled circles, large Kp ($> 2$) by triangles. Dotted line is both Kp's put together. All nightside MLT sectors (18-06) and both sunlit and darkness conditions are included.

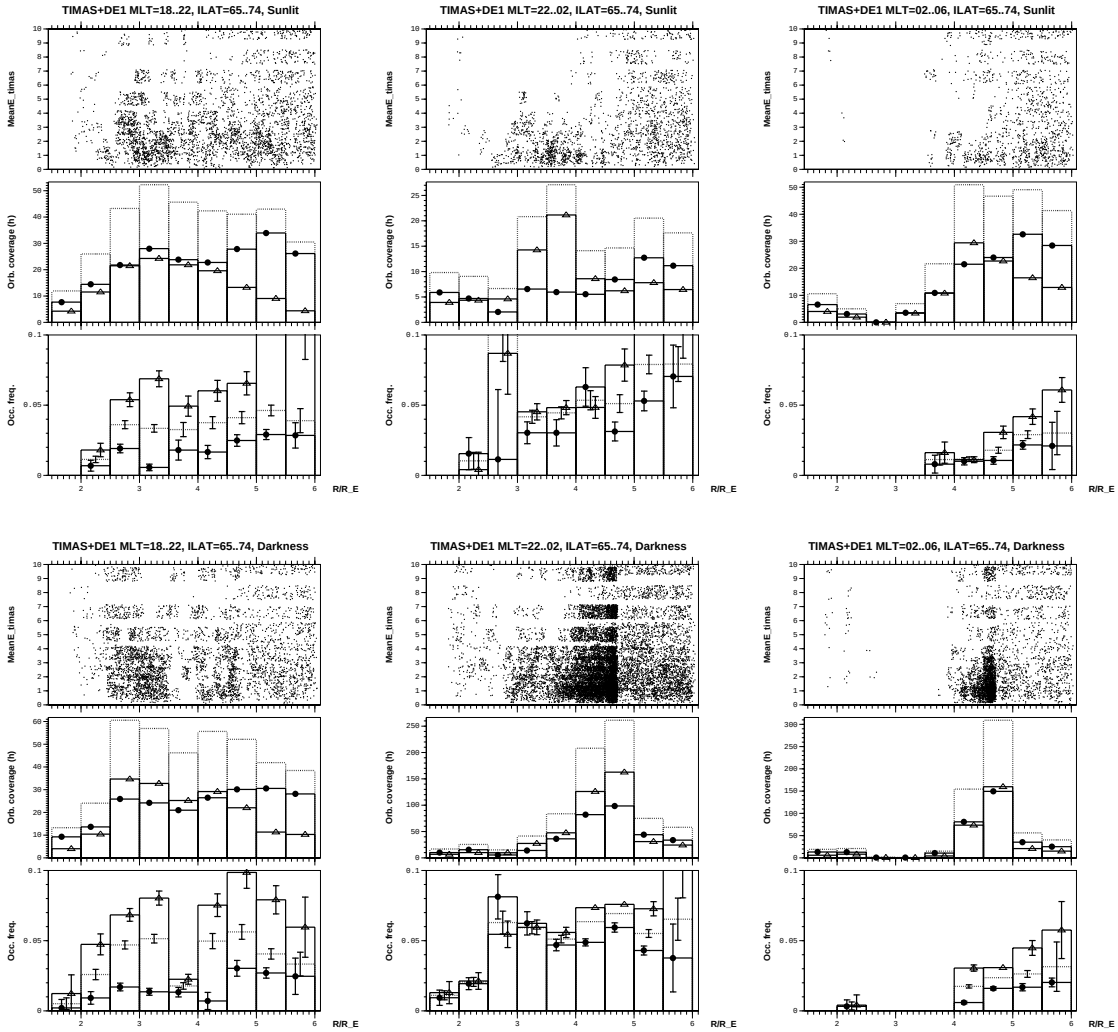


Figure 4: Same as Figure 3, but separated in the three nightside MLT sectors and sunlit (top) and darkness (bottom) conditions.

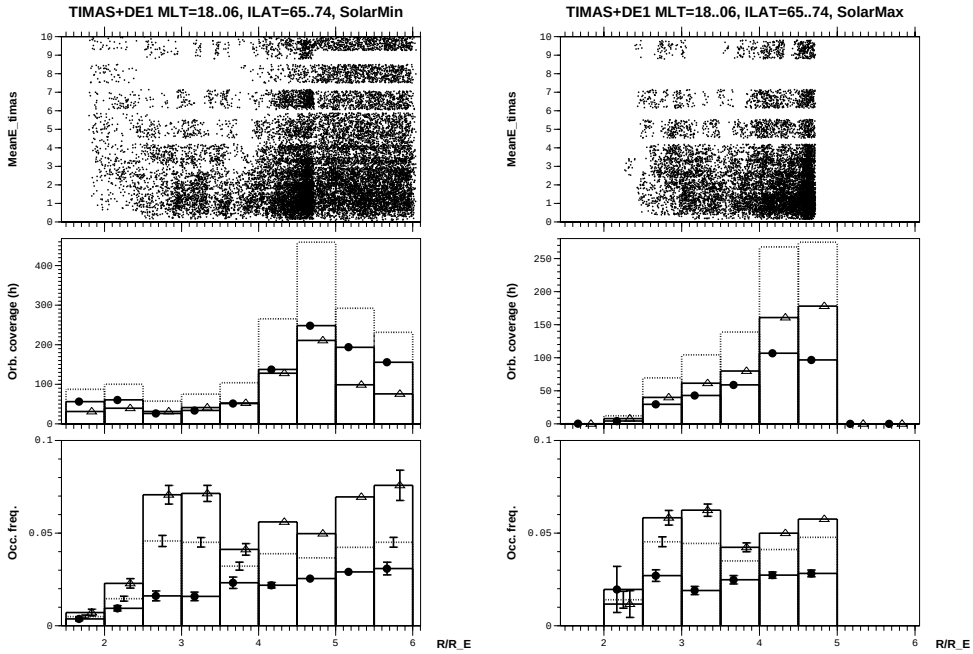


Figure 5: Same as Figure 3 but separated for solar minimum (left) and solar maximum years (right).

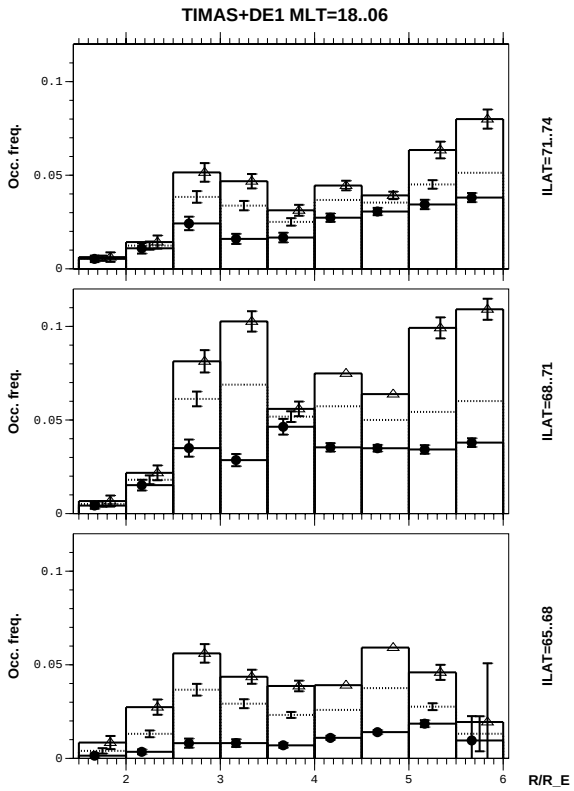


Figure 6: Same as the bottom panel of Figure 3 but shown separately for the ILAT ranges 71-74 (top), 68-71 (middle) and 65-68 (bottom).

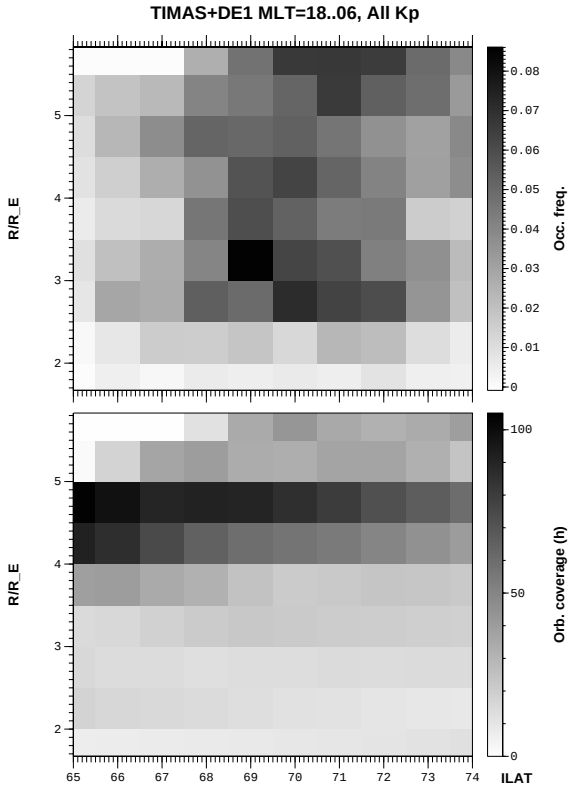


Figure 7: Top: Occurrence frequency of all nightside 0.5-10 keV ion beams as a function of ILAT and radial distance $R$. Bottom: Orbital coverage in hours in each bin. Both TIMAS and EICS data are put together. The dayside MLT range 10-14 may contain data errors and should not be looked at.

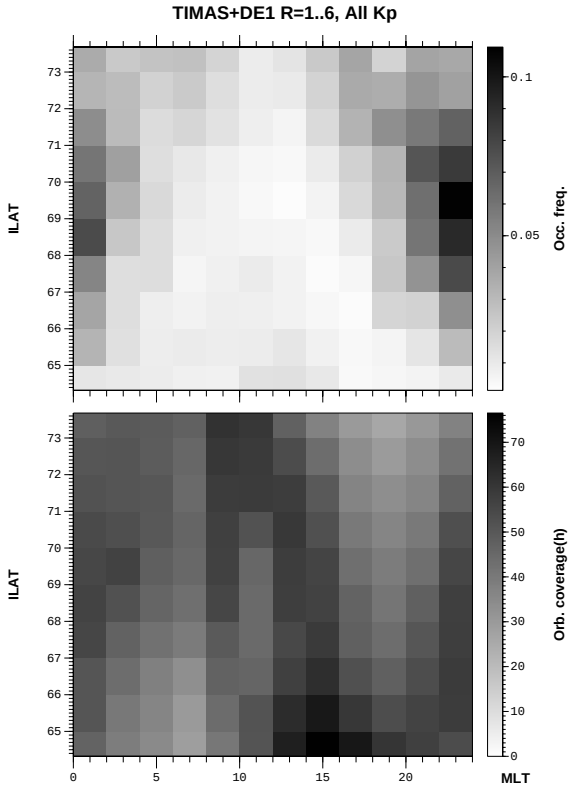


Figure 8: Top: Occurrence frequency of all 0.5-10 keV ion beams as a function of MLT and ILAT for all radial distances smaller than 6 $R_E$. Bottom: Orbital coverage in hours in each bin. Both TIMAS and EICS data are put together. The dayside MLT range 10-14 may contain data errors and should not be looked at.

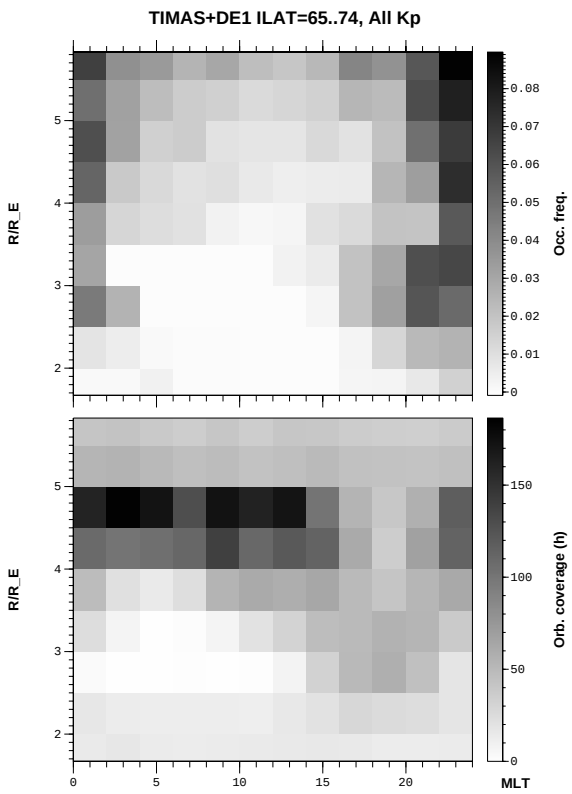


Figure 9: Top: Occurrence frequency of all 0.5-10 keV ion beams as a function of MLT and radial distance $R$ for all ILAT in the range 65..74. Bottom: Orbital coverage in hours in each bin. Both TIMAS and EICS data are put together.

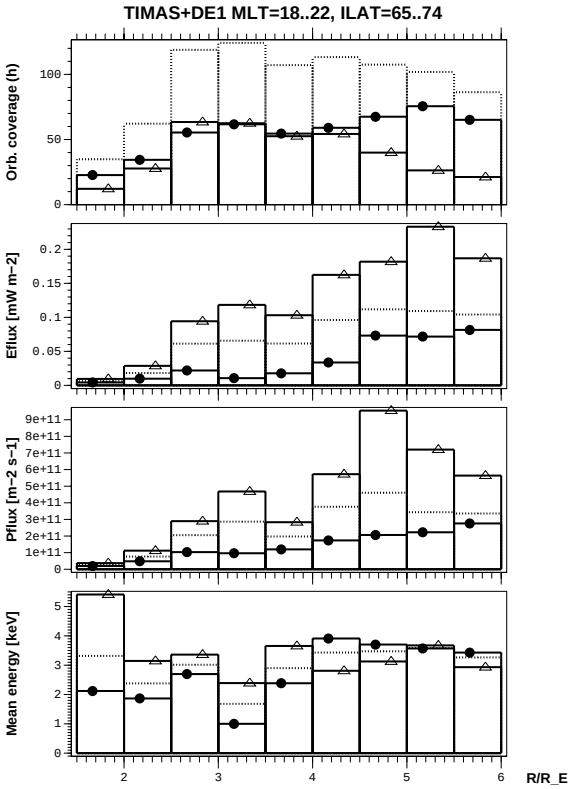


Figure 10: Top: Orbital coverage in hours in the evening MLT sector. Second panel: Average invariant energy flux (i.e., projected to ionospheric altitude) carried by upward ion beams. Third panel: Average invariant particle flux carried by beams. Fourth panel: Mean energy of beams, as weighted average over beams, weighting each beam by its particle flux.